Drug Occupancy Assessment at the Glucose-Dependent Insulinotropic Polypeptide Receptor by Positron Emission Tomography

Olof Eriksson,[1,2] Irina Velikyan,[2,3] Torsten Haack,[4] Martin Bossart,[4] Andreas Evers,[4] Katrin Lorenz,[4] Iina Laitinen,[4] Philip J. Larsen,[5] Oliver Plettenburg,[6] Lars Johansson,[1] Stefan Pierrou,[1] and Michael Wagner[4]

Diabetes 2021;70:842–853 | https://doi.org/10.2337/db20-1096

TECHNOLOGICAL ADVANCES

Targeting of the glucose-dependent insulinotropic polypeptide receptor (GIPR) is an emerging strategy in antidiabetic drug development. The aim of this study was to develop a positron emission tomography (PET) radioligand for the GIPR to enable the assessment of target distribution and drug target engagement in vivo. The GIPR-selective peptide S02-GIP was radiolabeled with ^{68}Ga. The resulting PET tracer [^{68}Ga]S02-GIP-T4 was evaluated for affinity and specificity to human GIPR (huGIPR). The in vivo GIPR binding of [^{68}Ga]S02-GIP-T4 as well as the occupancy of a drug candidate with GIPR activity were assessed in nonhuman primates (NHPs) by PET. [^{68}Ga]S02-GIP-T4 bound with nanomolar affinity and high selectivity to huGIPR in overexpressing cells. In vivo, pancreatic binding in NHPs could be dose-dependently inhibited by coinjection of unlabeled S02-GIP-T4. Finally, subcutaneous pretreatment with a high dose of a drug candidate with GIPR activity led to a decreased pancreatic binding of [^{68}Ga]S02-GIP-T4, corresponding to a GIPR drug occupancy of almost 90%. [^{68}Ga]S02-GIP-T4 demonstrated a safe dosimetric profile, allowing for repeated studies in humans. In conclusion, [^{68}Ga]S02-GIP-T4 is a novel PET biomarker for safe, noninvasive, and quantitative assessment of GIPR target distribution and drug occupancy.

The glucose-dependent insulinotropic polypeptide (GIP) (also known as the gastric inhibitory polypeptide) is an incretin hormone released from the intestinal K cells in response to nutrient intake with the main effect of stimulating insulin secretion from the β-cells through the GIP receptor (GIPR) (1). The GIPR is a transmembrane protein belonging to the class B G-coupled receptor family. Apart from its role in β-cell function, the GIPR has been associated not only with lipolysis but also with centrally mediated effects, including appetite control, which have been a source of controversy (1–4). Targeting of the GIPR is thus an emerging strategy in antidiabetic drug development (e.g., as part of dual- and trimodal peptide agonists also engaging the glucagon-like peptide 1 receptor [GLP-1R] and/or the glucagon receptor [GCGR]) (5–10). Clinical benefits of such unimolecular constructs may include, for example, improved glycemic control and weight reduction. However, it is difficult to elucidate the effects of such drug candidates mediated specifically by the GIPR because of its overlapping pharmacology with the GLP-1R as well as potentially the GCGR. It is a challenge to even demonstrate clear, unequivocal in vivo drug target engagement at the GIPR for these same reasons.

Previously, we have developed positron emission tomography (PET) radioligands for the GLP-1R and the GCGR for in vivo assessment of target distribution and drug target engagement. [^{68}Ga]DO3A-VS-Cys^{40}-Exendin-4 binds specifically to the GLP-1R and has enabled quantitative studies of GLP-1 drug occupancy in the pancreas in large animals (11,12) and humans (13). Similarly, the

[1]Antaros Medical AB, Mölndal, Sweden
[2]Science for Life Laboratory, Department of Medicinal Chemistry, Uppsala University, Uppsala, Sweden
[3]PET Centre, Centre for Medical Imaging, Uppsala University Hospital, Uppsala, Sweden
[4]Sanofi-Aventis Deutschland GmbH, Frankfurt, Germany
[5]Bayer Pharmaceuticals, Wuppertal, Germany
[6]Helmholtz Zentrum München, Munich, Germany

Corresponding authors: Michael Wagner, michael.wagner@sanofi.com, and Olof Eriksson, olof.eriksson@antarosmedical.com

Received 28 October 2020 and accepted 17 January 2021

This article contains supplementary material online at https://doi.org/10.2337/figshare.13607261.

GCGR-specific radiolabeled peptide [^{68}Ga]DO3A-VS-Cys^{40}-Tuna-2 was used to demonstrate drug target engagement in nonhuman primates (NHPs) (14,15) and humans (13). Thus, development of a similar radioligand but for the human GIPR (huGIPR) would enable direct quantification of in vivo dual/trimodal agonist target engagement on the GIPR, GLP-1R, and GCGR separately.

The GIPR has also been described as a potential imaging biomarker for detection of pancreatic and gastrointestinal neuroendocrine tumors (NETs) (16,17). NETs are often indolent and slow growing and may avoid detection by established cancer imaging diagnostics, such as [^{18}F] fluorodeoxyglucose PET. Interestingly, most NETs express GIPR, GLP-1R, or somatostatin receptor (18). PET radiodiagnostica are already established for somatostatin receptor (19–21) and GLP-1R (22–24). Development of a PET radioligand selective for GIPR would thus complete the coverage, thereby potentially enabling detection and localization of virtually all NETs. However, putative GIPR-selective radioligands are so far only available in the preclinical setting (25,26). Additionally, those ligands bound to huGIPR with a weaker potency than endogenous GIP (1–30) or GIP (1–42) when radiolabeled with ^{111}In or ^{68}Ga. While the radioligands visualized implanted xenograft tumors overexpressing the GIPR, none was described as useful for imaging the GIPR in pancreas, where overall receptor density is rather low. The aim of the current study was to develop a high-affinity PET radioligand for the GIPR to enable assessment of target distribution as well as drug target engagement in vivo in animals, as demonstrated here, and potentially in humans.

RESEARCH DESIGN AND METHODS

Peptide Discovery and Chemistry

The GIPR-selective ligand was developed by rational design on the basis of the structure of GIP (1–30) (Fig. 1). Compared with GIP (1–30), 10 amino acids were exchanged to increase affinity toward the huGIPR and to stabilize the peptide structure. An additional lysine was added to the C-terminus of the peptide, serving as an attachment point for the 1,4,7,10-tetraazacyclododecane-1,4,7,10-tetraacetic acid (DOTA) chelator moiety. DOTA was attached by amide coupling to the side chain amino group of that lysine in position 31.

Radiochemistry

The resulting DOTA-conjugated construct S02-GIP-T4 was radiolabeled with ^{68}Ga. The top fraction of $^{68}GaCl_3$ (3.5 mL, 0.1 mol/L with respect to hydrochloric acid) was eluted from a ^{68}Ge/^{68}Ga generator (GalliaPharm; Eckert & Ziegler, Berlin, Germany). The pH of the eluate was adjusted to 4.6–5.0 by sodium acetate buffer (1 mol/L, 300 μL) containing sodium hydroxide (30 μL, 10 mol/L). To suppress the radiolysis and improve solubility, ethanol (200 μL) and gentisic acid (300 μL, 0.032 mol/L) were added to the reaction mixture. Then, 15 nmol of the precursor (S02-GIP-T4) dissolved in acetate buffer (pH 7.0–7.4) were added. The reaction mixture was heated at 75°C for 10–15 min. The crude product was purified using a solid phase extraction cartridge (Oasis HLB). The product was eluted with 1 mL of 60% ethanol solution (pH 7). The final product was formulated dependent on the biological assay. Radiochemical purity and peptide content were determined by an ultraviolet (UV) radio-high-performance liquid chromatography autoanalyzer (LaChrom; VWR Hitachi) equipped with a reversed-phase analytical column (50 × 4.6 mm, particle size 3 μm) (C-4; Vydac) using mobile phases of A = 10 mmol/L trifluoroacetic acid and B = acetonitrile/10 mmol/L trifluoroacetic acid; linear gradient elution of 0–5 min from 20 to 45% B, 5–7 min 45% B, and 7–10 min from 45 to 80% B; and flow rate of 1.0 mL/min, with UV detection at 220 nm. Typical radiochemical purity was >98%. Data acquisition and handling were performed using the EZChrom Elite software package. The stability of the product at room temperature in 50% ethanol was monitored for 1–3 h and assessed by UV radio-high-performance liquid chromatography.

Chemicals

All chemicals and buffers were sourced from VWR Life Sciences Sweden, unless otherwise noted. Peptides (S02-GIP-T4, triple agonist 12 [TA12], GIP [1–42], GLP [7–36] NH_2) were synthesized at Sanofi according to well-described procedures (27).

In Vitro Potency Assay

The potency of S02-GIP-T4 as well as [Ga]S02-GIP-T4 (S02-GIP-T4 loaded with nonradioactive gallium) was assessed by a functional cAMP assay in HEK293 cells transfected with huGIPR, cynomolgus NHP, or rat GIPR (Sanofi). Details of the assay procedure are given in detail in the Supplementary Material and have been described previously (14,28).

Cell Affinity and Binding Specificity Assay

Affinity of the tracer was assessed using a saturation binding assay with the radiolabeled tracer [^{68}Ga]S02-GIP-T4. A displacement assay using the tracer labeled with stable gallium [Ga]S02-GIP-T4 was also performed (see Supplementary Material for details).

Affinity of [^{68}Ga]S02-GIP-T4 was assessed by in vitro autoradiography saturation binding studies on 20-μm sections of frozen pellets of huGIPR-HEK293 cells. GLP-1R–overexpressing cells (huGLP1R-HEK293) were used as negative control. Sections of huGIPR-HEK293 cell pellets were incubated over a range of concentrations of [^{68}Ga] S02-GIP-T4 (0.03–30 nmol/L) around the expected K_d. The sections were incubated (PBS, pH 7.4, 1% BSA, 25°C, 60 min) with radiotracer alone or in the presence of 10 μmol/L GIP (1–42) to block GIPR and assess nonspecific binding. After incubation, the sections were washed three times for 1 min, first with assay buffer and then twice with PBS. The sections were dried and then exposed to digital phosphorimager plates from at least two

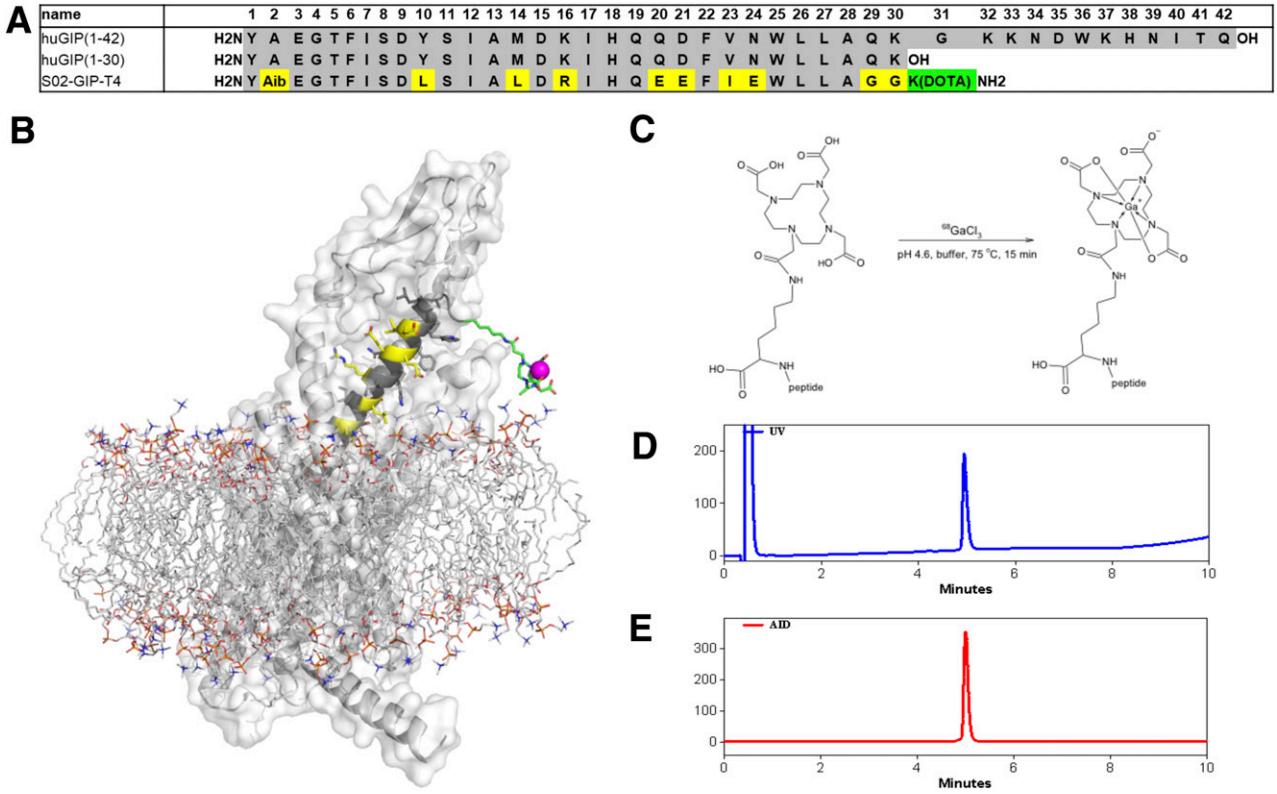

Figure 1—Structure and radiolabeling of GIPR-selective ligand S02-GIP-T4. Amino acid sequence for huGIP (1–42), huGIP (1–30), and S02-GIP-T4 (*A*). Model of [^{68}Ga]S02-GIP-T4 binding to the full-length huGIPR (*B*). ^{68}Ga labeling synthesis scheme presenting the structure of S02-GIP-T4 with the DOTA chelator moiety conjugated to the peptide through a C-terminal lysine amino acid residue (*C*). Typical UV radiochromatogram of a [^{68}Ga]S02-GIP-T4 preparation with UV trace (*D*) and radio trace (*E*), demonstrating >99% radiochemical purity. Aib, 2-Aminoisobutyric acid.

half-lives (2 h) to overnight. A reference droplet of 10 μL of assay buffer with radioactivity, cross-calibrated against a γ-counter, was included to enable quantification of the autoradiograms. The affinity assay was repeated three times.

Autoradiograms were analyzed in ImageJ, and binding data were converted to fmol/mm^3 by the internal reference and the specific radioactivity of the radiotracer batch (MBq/nmol). Specific binding was determined by subtracting nonspecific binding from total binding. Calculation of K_d and B_{max} was performed within each experiment using nonlinear curve fitting in GraphPad Prism 6.05 (GraphPad Software, La Jolla, CA).

Binding specificity was evaluated by incubating sections of huGIPR-HEK293 and huGLP1R-HEK293 cell pellets with ~5 nmol/L [^{68}Ga]S02-GIP-T4 (n = 5), using the same conditions as described above for the affinity assessment. The sections were incubated with [^{68}Ga]S02-GIP-T4 alone or with 10 μmol/L unlabeled S02-GIP-T4 precursor, 5 μmol/L GIP (1–42), or 1 μmol/L GLP (7–36)NH_2. Autoradiograms were obtained and analyzed as described above.

Animal Studies

National and institutional guidelines for the care and use of all animals (rats and cynomolgus NHPs) used in this study were followed. All procedures involving animals in this study were approved by the Animal Research Ethical Committee of the Uppsala Region and were performed according to Uppsala University guidelines on animal experimentation (UFV 2007/724).

Rat In Vivo Distribution

The organ distribution study in rat was performed to calculate the residence time for dosimetry. Thus, measurements at more time points were prioritized over repetitions at individual time points. In vivo organ distribution of [^{68}Ga]S02-GIP-T4 was evaluated in Sprague Dawley rats (Taconic Biosciences, Laven, Denmark) (n = 16, 277 ± 9 g, male). The animals were kept at a constant temperature (25°C) and humidity (50%) in a 12-h light-dark cycle. Food and water were provided ad libitum. Conscious animals were administered [^{68}Ga]S02-GIP-T4 (1.8 ± 0.6 MBq/kg in a maximum volume of 0.7 mL PBS, pH 7.4, corresponding to 1.0 ± 0.2 μg/kg) as a bolus in the tail vein. Two animals each were euthanized (gradually increasing the CO_2 content up to 80% for 1 min, followed by heart puncture) at eight time points after [^{68}Ga]S02-GIP-T4 administration (5, 10, 20, 40, 60, 90, 120, and 180 min). Tissues (blood, heart, lung, liver, pancreas, spleen, adrenal, kidney, small intestine [without/with its content], large intestine [without its content], feces, urinary bladder

[rinsed], testis/ovary, muscle, bone, bone marrow, thyroid, and brain) were immediately excised postmortem and measured for weight and radioactivity (Wallac γ-counter). The [^{68}Ga]S02-GIP-T4 uptake in all tissues was corrected for weight and radioactivity decay to the time point of administration and expressed as standardized uptake values (SUVs).

NHP Dose Escalation and Occupancy Studies

A dedicated drug-naive colony of lean, healthy NHPs was used for this study ($n = 6$, females, weight 4.0–6.3 kg). The housing as well as the handling, anesthesia, and monitoring of the NHPs during the PET studies are described in detail in the Supplementary Material.

[^{68}Ga]S02-GIP-T4 was evaluated for binding to the GIPR in pancreas by a dose escalation study design. Briefly, increasing doses of unlabeled precursor peptide S02-GIP-T4 were coinjected with [^{68}Ga]S02-GIP-T4 to demonstrate a dose-dependent blocking of the pancreatic signal. The rationale behind the design is described in the Supplementary Material.

For each scan, the animal was positioned to include the abdomen in the field of view of a Discovery MI PET/computed tomography (CT) scanner (GE Healthcare, Milwaukee, WI) by assistance of a low-dose CT scout view (140 kV, 10 mA). Attenuation correction was acquired by a 140-kV, Auto-mA 10–80 mA CT examination. [^{68}Ga]S02-GIP-T4 was administered intravenously, and the animal was examined in list mode by a dynamic PET protocol for 90 min (33 frames; 12 × 10 s, 6 × 30 s, 5 × 120 s, 5 × 300 s, 5 × 600 s). Image acquisition was performed in three dimensions and reconstructed using an iterative algorithm (Q.Clear β 200, 256 × 256 matrix, zoom 30-cm diameter). Discrete venous sampling was performed for measurement of radioactivity in whole blood and plasma by a well counter (5, 30, 60, and 90 min). Venous samples for assessment of endogenous GIP levels were acquired before and after [^{68}Ga]S02-GIP-T4 administration (P-800 tubes, −5 and 60 min).

For the dose escalation study, the PET examinations were repeated up to two times during each experimental day, with an increasing amount of administered radioactivity and coinjected S02-GIP-T4 peptide mass (Table 1). The scans were performed 3 h apart to allow for excretion and decay of the residual radiotracer from the prior scan. [^{68}Ga]S02-GIP-T4 dose escalation PET/CT studies were performed in five NHPs (Table 1).

The dose of [^{68}Ga]S02-GIP-T4 judged to induce minimum peptide mass effect (i.e., a tracer dose) was determined on the basis of the results of the dose escalation study. [^{68}Ga]S02-GIP-T4 (at doses <0.1 μg/kg) was then used to assess the occupancy of the candidate drug TA12.

[^{68}Ga]S02-GIP-T4 PET/CT scanning of the pancreas was performed at baseline and after subcutaneous administration of 50 μg/kg of study drug TA12 (4,935.6 g/mol, 10.1 nmol/kg), a TA with high activity at the GIPR (see Table 1). The discovery and characteristics of TA12 have been described in detail previously (27). The follow-up PET/CT scan was performed at T_{max} (≈2 h) for the study drug. Plasma pharmacokinetic samples were acquired before and up to 3.5 h after TA12 administration. GIPR occupancy studies were performed in three NHPs (Table 1).

Stability in Blood Plasma

The in vitro stability of [^{68}Ga]S02-GIP-T4 in plasma from three NHPs was assessed before and after 15, 45, or 90-min incubation (see Supplementary Material for detailed procedure).

NHP PET Data Analysis

The reconstructed PET data were analyzed using PMOD version 3.7 software (PMOD Technologies, Zurich, Switzerland). The following tissues were delineated for biodistribution and dosimetry assessment: liver, spleen, pancreas, kidney, descending aorta, muscle (*erector spinae*), heart, lung, intestine, cortical bone, and urinary bladder. Regions of interest were delineated on coregistered CT slices or directly on PET images. Regions of interest were delineated on transaxial sequential slices and combined into volumes of interest. Single voxels within the lumen were selected for delineation of the descending aorta.

The PET measurements were expressed as SUVs for the assessment of biodistribution. Patlak graphical analysis (29), which assumes irreversible binding, was selected for kinetic analysis because ^{68}Ga tends to residualize (i.e., become trapped) inside the cell. The net uptake rate (mL/cm^3/h) (i.e., the flux of tracer from blood into tissue) was estimated using dynamic PET data of the pancreas as output and a corrected aortic image-derived time-activity curve as input. The linear slope at some part of the PET examination (after linearization of the tissue and blood pool input) is identical to the net uptake rate. The existence of a net uptake rate in one part of the examination indicates that an irreversible process is occurring.

For each examination, the image-derived input curve (from descending aorta) was corrected by the individual plasma-to-whole blood ratio (on average 1.56 ± 0.17) and the metabolic stability of [^{68}Ga]S02-GIP-T4 in NHP plasma (population mean, assessed in vitro). The percentage of intact [^{68}Ga]S02-GIP-T4 was 98.7% after 15 min, 96.3% after 45 min, and 93.0% after 90 min compared with 99.5% intact at the end of synthesis. The metabolism of [^{68}Ga]S02-GIP-T4 during the first 90 min could be approximated as linear with a $k = -0.073$. Calculation of net uptake rate was performed using Excel software (Microsoft Corporation).

Human Predicted Dosimetry

The predicted dosimetry in humans was estimated on the basis of the biodistribution of [^{68}Ga]S02-GIP-T4 in rats (organ distribution study) and NHPs (six PET/CT studies at baseline tracer doses <0.1 μg/kg), as described previously (14,30). Briefly, the assessment of the residence

Table 1—Overview of the [^{68}Ga]S02-GIP-T4 PET/CT dose escalation and drug target occupancy studies in NHPs

			Scan 1		Scan 2		Scan 3	
Study type	NHP identifier	Weight (kg)	μg/kg	MBq/kg	μg/kg	MBq/kg	μg/kg	MBq/kg
Dose escalation	1	6.3	0.028	0.2	59.7	6.2	NA	NA
	2	4.0	0.034	0.3	53.0	11.3	NA	NA
	3	5.6	0.031	0.3	58.8	7.9	NA	NA
	4	4.3	0.081	0.8	0.49	1.2	2.5	1.5
	5	4.3	0.15	1.4	1.1	1.7	7.6	2.9

			Scan 1		Intervention	Scan 2	
	NHP identifier	Weight (kg)	μg/kg	MBq/kg	μg/kg TA12	μg/kg	MBq/kg
Occupancy	2	4.2	0.046	0.5	50	0.022	0.3
	3	5.3	0.033	0.4	50	0.021	0.3
	6	4.1	0.041	0.4	50	0.03	0.4

NA, not applicable.

times of the PET tracer was preceded by the normalization of the SUV data in the various tissues of rat or NHP (SUV_A) to the whole-body adult reference phantom weights (31). This was performed according to the following equation:

$$\left[\frac{\%}{\text{organ}}\right]_{\text{human}} = \text{SUV}_\text{A} \times \left(\frac{\text{g}_\text{organ}}{\text{kg}_\text{weight}}\right)_{\text{human}}$$

The decay-corrected and normalized SUVs were back corrected to count rates to calculate the actual radiation burden in each tissue. The residence times (MBq-h/MBq) of the respective PET tracer in various tissues were assessed by trapezoidal approximation of the collected kinetic data followed by the extrapolation of the remaining points from the last time point to infinity by a single monoexponential fit. Bone marrow residence times were assessed according to the bone marrow blood model.

The estimation of the absorbed dose was performed by OLINDA/EXM version 1.1 software, where the calculations were based on the adult reference male or female phantom to obtain the intended absorbed dose estimate in humans (International Commission on Radiological Protection 60). The organ-specific and effective doses are reported as mSv/MBq. The amount of MBq of [^{68}Ga]S02-GIP-T4 that can be administered annually (MBq/year) was calculated for each organ, as well as the effective dose, by dividing the acceptable localized dose for each tissue (150 mSv/year for most tissues, 50 mSv for some radiosensitive tissues) by the dose (mSv/MBq).

Statistics

Group-level data are reported as mean ± SD. Statistical analysis was performed using GraphPad Prism 8 software, and differences were assessed by Student *t* test using a significance level of $P < 0.05$.

Data and Resource Availability

The data that support the findings of this study are available from Sanofi, but restrictions apply to the availability of these data, which were used under license for the current study and therefore are not publicly available. Data are available, however, from the authors upon reasonable request and with permission of Sanofi.

RESULTS

Radiochemistry

[^{68}Ga]S02-GIP-T4 (Fig. 1*A*) ($n = 14$) was synthesized with a nondecay-corrected radiochemical yield of 54.2 ± 3.5% and a specific radioactivity of 66.2 ± 12.0 MBq/nmol. The radioactivity at end of synthesis was 620 ± 126 MBq, with a radiochemical purity of 99.9 ± 0.1% (Fig. 1*B* and *C*).

Potency, Affinity, and Binding Assay

S02-GIP-T4 as well as [Ga]S02-GIP-T4 (S02-GIP-T4 loaded with stable, nonradioactive gallium) selectively activated the huGIPR with potencies of half-maximal effective concentration (EC_{50}) (cAMP) = 1.1 pmol/L (Table 2). The binding affinity of the tracer chelated with stable gallium [Ga]S02-GIP-T4 was assessed in a displacement assay with [^{125}I]GIP using membranes from huGIPR-HEK293 cells. Here, [Ga]S02-GIP-T4 inhibited binding of [^{125}I]GIP to huGIPR with an IC_{50} of 0.25 nmol/L compared with 3.1 nmol/L for native GIP (1–42), showing an increased binding affinity toward native GIP of at least 10-fold (data not shown).

The binding affinity of radiolabeled [^{68}Ga]S02-GIP-T4 toward huGIPR was on average $K_d = 0.87 \pm 0.11$ nmol/L (on the basis of three different experiments) (Fig. 2*A* and *B*). [^{68}Ga]S02-GIP-T4 bound specifically to the huGIPR with low background binding because binding to huGIPR-HEK293 was abolished by coincubation with either GIP (1–42) or S02-GIP-T4 (the unlabeled precursor peptide) but not with GLP (7–36)NH_2 (Fig. 2*C* and *D*). There were only negligible interactions with the GLP-1R when studying the binding to huGLP1R-HEK293 cells. [^{68}Ga]S02-GIP-T4 showed generally low binding, and there was no reduced binding when coincubating with GLP (7–36)NH_2.

Rat In Vivo Biodistribution

Organ distribution kinetics were examined in Sprague Dawley rats ($n = 16$) that had received [^{68}Ga]S02-GIP-T4. Low

Table 2—Potencies of S02-GIP-T4 and [Ga]S02-GIP-T4 at the GIPR from human, rat, and NHP in transfected HEK293 cells compared with GIP (1–42)

	Human			Rat			NHP		
Peptide	EC_{50} GIPR (pmol/L)	EC_{50} GLP-1R (pmol/L)	EC_{50} GCGR (pmol/L)	EC_{50} GIPR (pmol/L)	EC_{50} GLP-1R (pmol/L)	EC_{50} GCGR (pmol/L)	EC_{50} GIPR (pmol/L)	EC_{50} GLP-1R (pmol/L)	EC_{50} GCGR (pmol/L)
GIP (1–42)	0.48	>10,000	>10,000	0.81	>10,000	>10,000	0.42	>10,000	>10,000
S02-GIP-T4	1.13	>10,000	>10,000	4.37	>10,000	>10,000	2.65	>10,000	>10,000
[Ga]S02- GIP-T4	1.09	>10,000	>10,000	2.63	>10,000	>10,000	1.94	>10,000	>10,000

retention was seen in most tissues, except for excretion through the kidneys into the urine (Fig. 3*A*). The retention in pancreas increased over time compared with the blood pool (Fig. 3*B*).

NHP In Vivo Biodistribution

[^{68}Ga]S02-GIP-T4 biodistribution over 90 min was assessed by PET/CT scan in NHPs after intravenous administration of S02-GIP-T4 peptide in amounts corresponding to <0.15 μg/kg. The tracer exhibited rapid distribution into the blood pool followed by clearance from most tissues over the next 5 min (Fig. 3*C* and *D*). Strong uptake of [^{68}Ga]S02-GIP-T4 was noted in the liver as well as in the renal medulla/pelvis and urine. The pancreas also exhibited retention compared with, for example, the blood pool but a relatively low magnitude of uptake.

NHP Dose Escalation Study

The baseline uptake of [^{68}Ga]S02-GIP-T4 in pancreas was clearly visualized and higher compared with reference tissues in the abdomen, such as spleen (Fig. 4*A*). For high blocking doses, pancreas in contrast exhibited clearance similar to spleen (Fig. 4*B*). There was a tendency for a dose-dependent decrease in binding of [^{68}Ga]S02-GIP-T4 in pancreas on basis of the SUV analysis (i.e., high doses of competing unlabeled S02-GIP-T4 precursor resulting in lower pancreas uptake as assessed by SUV) (Fig. 4*C*). The blocking effect was clearly evident on a group-level analysis, where the SUV after coinjection with >2 μg/kg S02-GIP-T4 precursor peptide was decreased compared with baseline scans (Fig. 4*D*).

However, there was an overlap between the groups indicating that the sensitivity of the analysis should be improved by using more of the dynamic information compared with the SUV analysis (using just the last static 30 min of the examination). Patlak graphical analysis demonstrated linearization from ~30 min until 90 min after administration of [^{68}Ga]S02-GIP-T4 on PET examination (i.e., irreversible binding in pancreas during this time, indicating an active uptake process such as receptor-mediated binding and internalization). For spleen, a positive net uptake rate could not be calculated, indicating the absence of active binding in this tissue. The net uptake rate for all the examinations in the dose escalation study demonstrated a progressive decrease in [^{68}Ga]S02-GIP-T4 binding for coinjections of S02-GIP-T4 precursor peptide greater than ~0.1 μg/kg (Fig. 5*A*). Thus, in this scenario, administration of [^{68}Ga]S02-GIP-T4 corresponding to a peptide mass <0.1 μg/kg can be considered as baseline (i.e., tracer doses incurring low or negligible receptor occupancy).

The average net uptake rate of the baseline doses was 0.14 ± 0.02 mL/cm^3/h (n = 7). The background binding (i.e., where no further decrease in binding was observed despite additional coinjected S02-GIP-T4 precursor peptide) was ~0.025 mL/cm^3/h. The in vivo K_d (i.e., the dose resulting in 50% decrease of the baseline signal) was ~0.35 μg/kg in pancreas (Fig. 5*A*). On a group level, there was a clear reduction in binding of 76% from baseline (<0.1 μg/kg) when coinjecting peptide masses in excess of 2 μg/kg ($P < 0.0001$) (Fig. 5*B*). The GIPR occupancy induced by the coinjected S02-GIP-T4 precursor peptide was increasing with coinjected dose, reaching occupancies >80% for the higher doses (Fig. 5*C*). There was a correlation between the net uptake rate assessment and the $SUV_{60–90\ min}$ measurement ($R^2 = 0.45$, $P < 0.01$).

NHP Occupancy

To test the tracer's suitability for receptor occupancy assessment, we studied the effects of the triple GLP-1R/GCGR/GIPR agonist drug candidate TA12 with high GIPR activity on receptor occupancy in NHPs. Pretreatment with 50 μg/kg s.c. TA12 almost completely abolished the [^{68}Ga]S02-GIP-T4 signal in the pancreas (Fig. 5*D*). The decrease in the net uptake rate was, on average, 88.7 ± 7.9% (n = 3, $P < 0.01$) (Fig. 5*D*).

Human Predicted Dosimetry

The predicted absorbed radiation dose in human tissues was extrapolated from [^{68}Ga]S02-GIP-T4 biodistribution data in rat as well as NHP (Table 3). The absorbed dose was clearly highest in the kidney (0.47 mSv/MBq) on the basis of rat data. However, on the basis of NHP data, the heart wall (myocardium), kidney, and liver exhibited the highest absorbed doses (~0.12 mSv/MBq).

The limiting tissue on the basis of rat data was the kidney, which allows for 322 MBq [^{68}Ga]S02-GIP-T4 to be administered before reaching the annual kidney limit of 150 mSv. NHP data, on the other hand, allows for >1,200 MBq annually before reaching 150 mSv absorbed dose in

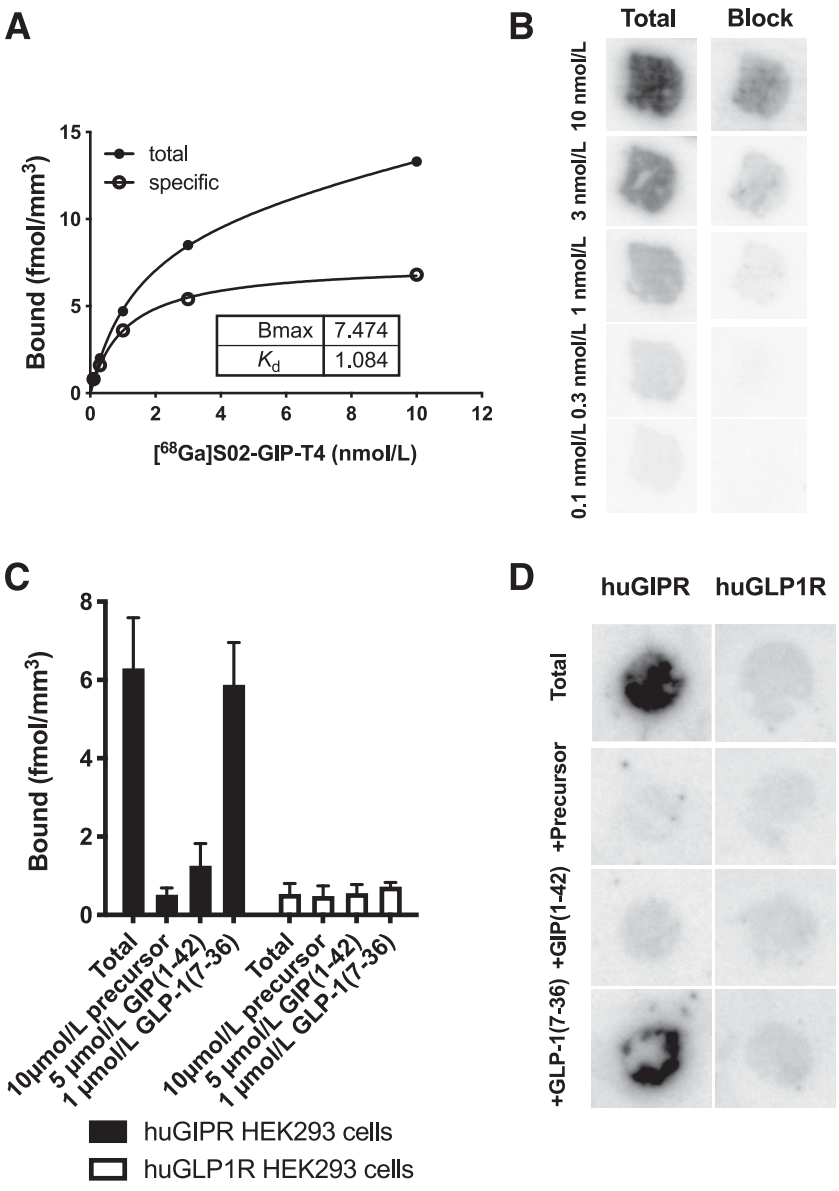

Figure 2— In vitro binding affinity and specificity of [^{68}Ga]S02-GIP-T4. Data from representative [^{68}Ga]S02-GIP-T4 saturation binding assay in huGIPR-HEK293 cells. The average affinity toward huGIPR was $K_d = 0.87 \pm 0.11$ nmol/L on the basis of three independent experiments (*A*). Autoradiograms of the sections in the experiment are also shown (*B*). Binding specificity toward GIPR was demonstrated in sectioned huGIPR-HEK293 and huGLP1R-HEK293 cells by incubation with [^{68}Ga]S02-GIP-T4 alone (total) of coincubation with S02-GIP-T4 (precursor), GIP (1–42), or GLP-1 (7–36)NH_2 (*C*). Representative autoradiograms from one of the experiments are shown (*D*).

the critical organs heart wall, kidney, and liver. The limiting individual tissue on the basis of NHP data are instead red marrow (bone marrow) because of the higher sensitivity to radiation (maximum 1,136 MBq annually to reach the limit of 50 mSv). However, the whole-body effective dose is even more limiting on the basis of NHP data, allowing for 446 MBq [^{68}Ga]S02-GIP-T4 annually.

DISCUSSION

Direct and quantitative PET imaging biomarkers for the GIPR would be of value for drug development and NET diagnostics. Here, we report the discovery, radiolabeling, and evaluation of a novel peptide ligand with high selectivity and subnanomolar affinity for the GIPR. The cross-reactivity for the GLP-1R was negligible, which is crucial since both GLP-1R and GIPR are expressed in the same target tissues.

Here, we demonstrate that [^{68}Ga]S02-GIP-T4 has sufficient sensitivity to enable in vivo imaging of GIPR in the pancreas. In the sparse literature on this topic, earlier described radioligands for the GIPR have mainly facilitated the visualization of xenografts (i.e., overexpressing lesions with nonphysiological levels of GIPR expression) (18,25,26). The performance of [^{68}Ga]S02-GIP-T4 is mainly due to the improved affinity to GIPR, which is a magnitude higher than for the previously reported

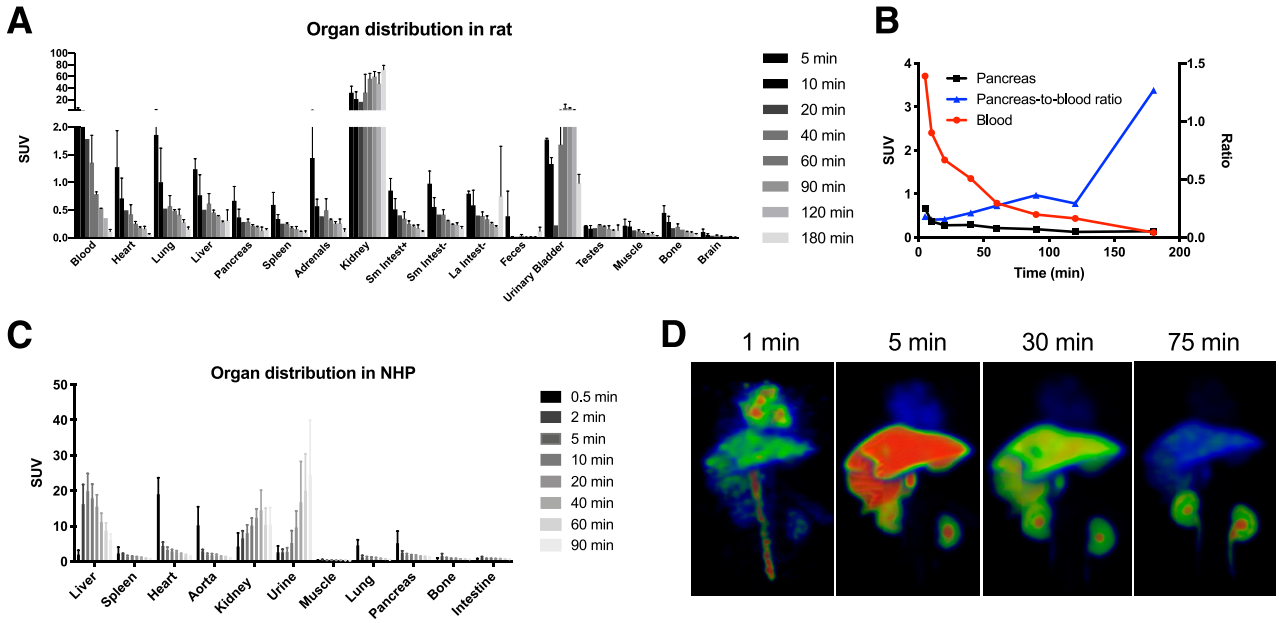

Figure 3—In vivo biodistribution of [^{68}Ga]S02-GIP-T4 in rat and NHP. [^{68}Ga]S02-GIP-T4 demonstrated fast biodistribution and rapid washout from most tissues except kidney and urinary bladder (*A*). The pancreas-to-blood ratio in rat increased with time (*B*). The biodistribution of [^{68}Ga]S02-GIP-T4 in NHPs ($n = 6$, average ± SD) (*C*). The color-coded images are three-dimensional projections of a representative NHP at different time points after [^{68}Ga]S02-GIP-T4 administration (*D*). The images are normalized to an SUV of 30 and directly comparable in intensity. La Intest–, large intestine without contents; Sm Intest+, small intestine with contents; Sm Intest–, small intestine without contents.

approaches. The binding potential (B_{max}/K_d) states that imaging of a certain level of receptor density (B_{max}) is linearly improved with the improvement of radioligand affinity (K_d).

[^{68}Ga]S02-GIP-T4 binding in pancreas could be dose dependently reduced by coinjection of unlabeled S02-GIP-T4 precursor peptide as well as abolished by pretreatment with TA12, a peptide drug candidate with high GIPR agonistic activity. This strongly suggests that the pancreatic binding is GIPR mediated.

GIP (1–42) blocked the binding of [^{68}Ga]S02-GIP-T4 in vitro. Thus, blocking with GIP (1–42) in vivo was also considered, but given the short biological half-life of endogenous GIP (1–42), an infusion regimen would probably be necessary. Such a study design would require keeping the [^{68}Ga]S02-GIP-T4 peptide mass constant for all studies, thus not being compatible with the dose escalation design that was used. Blocking [^{68}Ga]S02-GIP-T4 binding by GIP (1–42) infusion should be further explored in future clinical PET studies.

The pancreas uptake, expressed as SUV, was ~1.2 in magnitude after 60–90 min postadministration. The accumulation in pancreas is approximately sevenfold lower compared with, for example, the GLP-1R radioligand [^{68}Ga]DO3A-VS-Exendin-4 ($SUV_{60–90min}$ ≈8) (32).

[^{68}Ga]S02-GIP-T4 baseline and follow-up PET/CT scanning enabled for the first time the direct in vivo observation of drug target engagement of a GIPR agonist. Pretreatment with 50 μg/kg TA12 induced a strong decrease in pancreatic uptake of [^{68}Ga]S02-GIP-T4 by 88.7 ± 7.9%, which should be interpreted as a GIPR occupancy of almost 90%. This level of occupancy was expected from the applied high dose (50 μg/kg) at T_{max} (i.e., time for maximal plasma exposure) of this peptide drug candidate. The occupancy is furthermore in the range of the maximal decrease in binding observed in the dose escalation study, where coinjection of up to 60 μg/kg S02-GIP-T4 precursor peptide induced receptor occupancy of up to 82% (Fig. 5*C*). Static SUV measurements may be preferable to use because of the less complicated logistics involved in the PET/CT scanning protocol (shorter duration of the scan, less stress for the examined subject). However, the improved accuracy of the Patlak graphical analysis compared with the SUV analysis indicates that a full dynamic scan protocol, including blood sampling and metabolite analysis, is required for GIPR target engagement quantification in future clinical studies.

Apart from the incretin effect in pancreas, GIPR pharmacology has also been implicated in other tissues. These include centrally mediated effects (e.g., on appetite/satiety) potentially by GIPR in the area postrema and hypothalamus (33). Since these regions are partially outside of the blood-brain barrier, the GIPR population should theoretically be available for binding and consequent imaging by [^{68}Ga]S02-GIP-T4. However, separate dedicated dynamic brain studies using high-resolution PET scanners are likely required for accurate quantification and localization of GIPR imaging in specific central nervous system regions. GIPR has also been associated with adipose tissue (34) and bone metabolism (35). NHPs used in this study

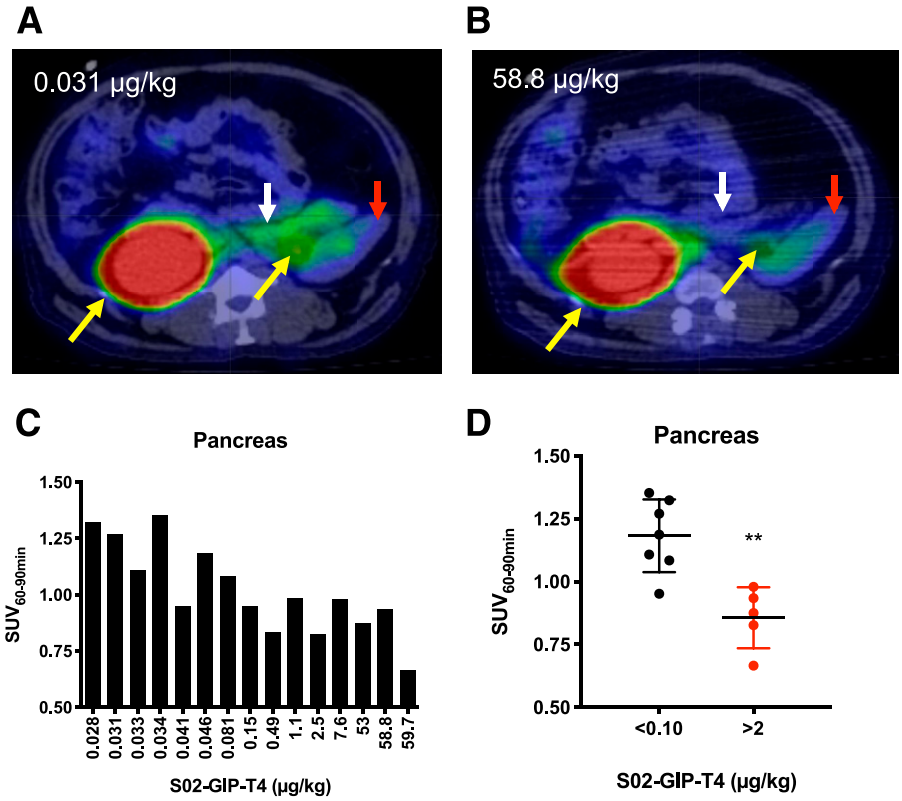

Figure 4—Visual and SUV analysis of pancreatic binding of [^{68}Ga]S02-GIP-T4 in NHP. Representative transaxial projections at the level of the pancreas of [^{68}Ga]S02-GIP-T4 at baseline (*A*) and after coinjection of a high dose of unlabeled S02-GIP-T4 precursor peptide for receptor blocking (*B*). White arrows indicate pancreas, red arrows indicate spleen, and yellow arrows indicate kidneys. Images are normalized to an SUV of 3 to allow direct comparison. The SUV values in pancreas from 60 to 90 min was high at baseline but decreased when S02-GIP-T4 precursor peptide was coinjected both individually (*C*) and on the group level (*D*). $^{**}P < 0.01$.

were quite lean, and thus, in combination with the use of a clinical PET scanner with ∼5-mm resolution, it would be difficult to delineate adipose tissue deposits without inducing significant partial volume effects (i.e., the PET pixel contains both the target tissue and the surrounding tissues, causing artificial dilution of the signal, directly confounding quantification). Separate studies in animal models of metabolic syndrome or even clinical studies in obese subjects are required to elucidate the possibility of GIPR quantification in different adipose tissue types.

[^{68}Ga]S02-GIP-T4 uptake, background binding, and washout in most tissues were similar in both rat and NHP. The route of excretion, on the other hand, surprisingly differed somewhat. In rat, the major route of excretion occurred through the kidney and into the urinary bladder. In NHP, on the other hand, strong uptake was also seen in the liver as was excretion through the renal medulla/pelvis into the urinary bladder but not with the common trapping of radionuclide in the cortex. This is rather unusual for ^{68}Ga-labeled peptides, which typically are trapped intracellularly in the renal cortex following reabsorption by the renal tubules. For many radiolabeled peptides, the liver usually shows relatively low uptake. The biodistribution pattern thus indicates that some form of metabolism of [^{68}Ga]S02-GIP-T4 is occurring. A potential mechanism could be metabolism in the liver (high uptake throughout the scan) followed by release of labeled metabolites into the blood stream. There is no evidence of biliary excretion into the intestine throughout the scan, which indicates that any [^{68}Ga]DOTA-conjugated peptides generated from hepatic metabolism are relatively hydrophilic since lipophilic peptides in liver cells have been shown to rapidly complex with bile salts and enter the intestine (36). The absence of radioactivity in the intestines or bile ducts thus strongly indicates that the radioactive peptide metabolites are hydrophilic. Instead, the main route of excretion of radioactivity was through the renal pelvis and further into the urinary bladder. Only limited retention was seen in the renal cortex in NHPs.

Because of the differing routes of excretion for [^{68}Ga]S02-GIP-T4 in rat and NHP, there was a corresponding species difference in the human predicted dosimetry. In rat, kidney was clearly the dosimetric critical organ tissue. In NHP, on the other hand, [^{68}Ga]S02-GIP-T4 exhibited strong uptake (SUV ≈10–20) in several tissues, including liver, kidney, and urine, but none of these tissues exhibited such high uptake in the renal cortex as in rat (SUV >50). Therefore, none of these tissues in NHP receive large

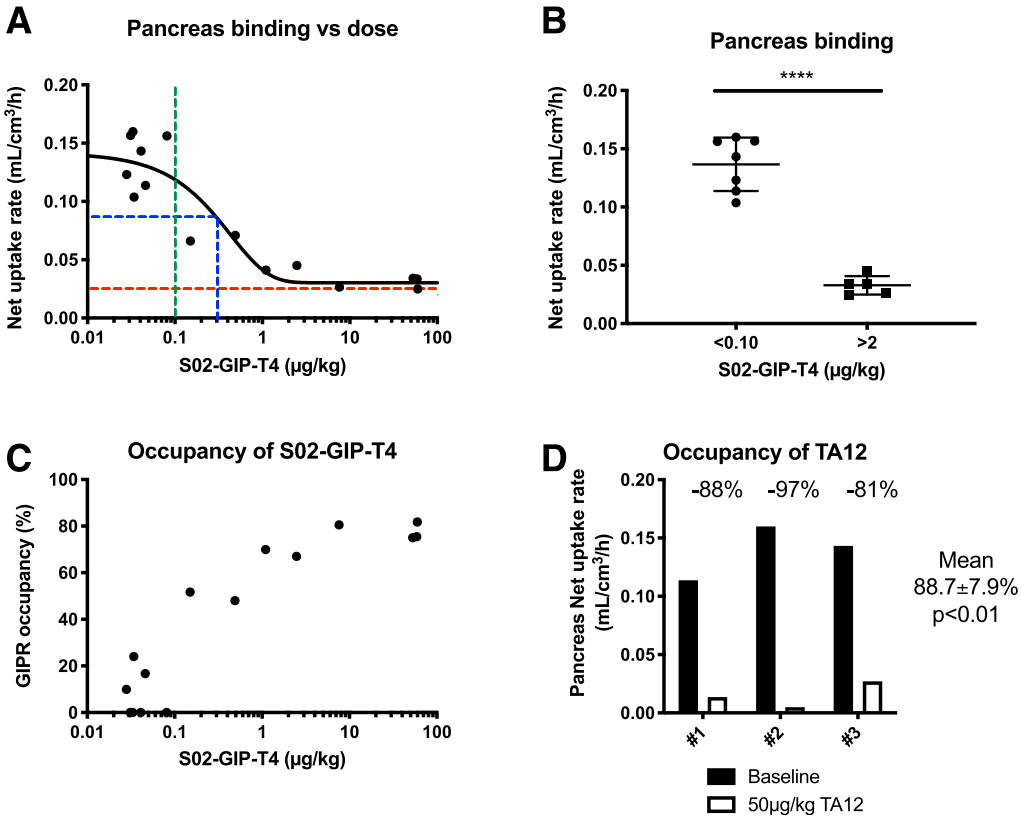

Figure 5—Quantitative analysis of NHP pancreas binding and occupancy assessment. Summary of Patlak graphical analysis of [^{68}Ga]S02-GIP-T4 for assessment of the net uptake rate for the examinations in the dose escalation study. Patlak-derived net uptake rate in pancreas is plotted against amounts of coinjected S02-GIP-T4 precursor peptide dose (*A*), where the green line indicates the range below which there was no obvious mass effect, the blue line indicates in vivo K_d, and the red line indicates the background binding. Coinjected S02-GIP-T4 precursor peptide doses >2 μg/kg reproducibly decreased the binding compared with baseline (*B*). Occupancy at GIPR induced by coinjected amount of S02-GIP-T4 precursor peptide mass (*C*). Decrease in [^{68}Ga]S02-GIP-T4, as assessed by Patlak-derived net uptake rate after pretreatment with 50 μg/kg TA12 compared with baseline in three independent experiments (*D*). ****$P < 0.0001$.

absorbed doses, and the whole-body effective dose is instead the limiting factor. Furthermore, the blood clearance was slower in NHP compared with rat, which resulted in a higher predicted absorbed dose to myocardium. The majority of the received dose in myocardium in the accepted dosimetry model is crossfire from passing blood in the circulation rather than actual uptake in the heart wall itself. Per previously described procedures (27), the blood pool data were used as proxy for red marrow since bone marrow is very difficult to delineate in PET images without having to accept severe partial volume effects. In fact, because of the higher radiosensitivity of red marrow (50 mSv annual maximal dose vs. 150 mSv for most other tissues), this tissue is the dose-limiting critical organ. Given the higher fidelity between NHP and human (compared with rat), it is likely that the NHP biodistribution and excretion patterns will translate better to the clinical situation. On the basis of the effective whole-body dose (calculated from the NHP data), humans may be administered up to 446 MBq annually before reaching 10 mSv, which is a common radiation safety limit in young adults. [^{68}Ga]S02-GIP-T4 can thus be administered repeatedly (at least two scans of 200 MBq each) also in humans, enabling baseline and follow-up studies of GIPR distribution and drug target engagement studies.

Dual agonists and TAs targeting the GLP-1R, GCGR, and GIPR are an exciting new field for a potential treatment of obesity and diabetes. The big unknown in this area is the optimal ratio of activation of the different receptors, which also might be different in the various species. At the same time, progress is currently hampered by a lack of quantitative biomarkers to adequately address this question. Having the new GIP tracer now available, which finally allows GIPR occupancy studies in preclinical species as well as in humans, the tool box, together with the available PET tracers for the GLP-1R and GCGR, is now complete to study this question in receptor occupancy studies through PET imaging.

In conclusion, [^{68}Ga]S02-GIP-T4 is a novel radiolabeled peptide ligand exhibiting high affinity and specificity for the GIPR, which enables assessment of drug interaction in pancreas in vivo. Additionally, it has a suitable biodistribution and dosimetry profile. [^{68}Ga]S02-GIP-T4 thus constitutes a novel PET biomarker for safe, noninvasive, and

Table 3—Human predicted dosimetry of [^{68}Ga]S02-GIP-T4 extrapolated from rat and NHP biodistribution data

Tissue	Dose from rat data (mGy/MBq)	Dose from NHP data (mGy/MBq)
Adrenals	0.00769	0.0092
Brain	0.000845	0.00119
Breasts	0.00155	0.00291
Gallbladder wall	0.0044	0.0113
Lower large intestine wall	0.00229	0.0205
Small intestine	0.00682	0.00995
Stomach wall	0.00303	0.0145
Upper large intestine wall	0.00315	0.0156
Heart wall	0.0766	0.117
Kidneys	0.465	0.116
Liver	0.00877	0.116
Lungs	0.00763	0.012
Muscle	0.00261	0.00539
Pancreas	0.00792	0.0214
Red marrow	0.0285	0.044
Osteogenic cells	0.0209	0.0425
Skin	0.000923	0.00165
Spleen	0.00797	0.014
Testes	0.00205	0.00112
Thymus	0.00362	0.00569
Thyroid	0.000806	0.00166
Urinary bladder wall	0.00378	0.0234
Effective dose (mSv/MBq)	0.0181	0.0224

The absorbed radiation dose in individual tissues and the whole-body effective dose are presented.

quantitative assessment of GIPR target distribution, drug occupancy, and NET diagnosis.

Acknowledgments. The authors thank Dr. Tim Klöckner (Sanofi) for testing relevant compounds in displacement assays with [^{125}I]GIP using membranes from huGIPR-HEK293 cells as well as Dr. Ziu Li (Sanofi) for testing relevant compounds in functional cAMP assays in HEK293 cells. The Preclinical PET/MRI Platform at Uppsala University is acknowledged for providing expertise, instrumentation, and facilities for PET tracer evaluation.

Duality of Interest. The study was sponsored in full by Sanofi. T.H., M.B., A.E., K.L., I.L., P.J.L., and M.W. are employees of Sanofi. L.J., S.P., and O.E. are employees of Antaros Medical AB. No other potential conflicts of interest relevant to this article were reported.

Author Contributions. O.E. and M.W. designed the study, researched data, analyzed data, and wrote the manuscript. I.V., T.H., M.B., A.E., K.L., I.L., O.P., and S.P. researched data, contributed to the data analysis, and reviewed the manuscript. P.J.L. and L.J. designed the study and reviewed the manuscript. O.E. is the guarantor of this work and, as such, had full access to all the data in the study and takes responsibility for the integrity of the data and the accuracy of the data analysis.

Prior Presentation. Parts of this study were presented at the 56th Annual European Association for the Study of Diabetes Virtual Meeting, 21–25 September 2020.

References

1. Seino Y, Fukushima M, Yabe D. GIP and GLP-1, the two incretin hormones: similarities and differences. J Diabetes Investig 2010;1:8–23
2. Finan B, Ma T, Ottaway N, et al. Unimolecular dual incretins maximize metabolic benefits in rodents, monkeys, and humans. Sci Transl Med 2013;5:209ra151
3. Mroz PA, Finan B, Gelfanov V, et al. Optimized GIP analogs promote body weight lowering in mice through GIPR agonism not antagonism. Mol Metab 2019;20:51–62
4. Killion EA, Wang J, Yie J, et al. Anti-obesity effects of GIPR antagonists alone and in combination with GLP-1R agonists in preclinical models. Sci Transl Med 2018;10:eaat3392
5. Bergmann NC, Lund A, Gasbjerg LS, et al. Effects of combined GIP and GLP-1 infusion on energy intake, appetite and energy expenditure in overweight/obese individuals: a randomised, crossover study. Diabetologia 2019;62:665–675
6. Lorenz M, Evers A, Wagner M. Recent progress and future options in the development of GLP-1 receptor agonists for the treatment of diabesity. Bioorg Med Chem Lett 2013;23:4011–4018
7. Finan B, Yang B, Ottaway N, et al. A rationally designed monomeric peptide triagonist corrects obesity and diabetes in rodents. Nat Med 2015;21:27–36
8. Kannt A, Madsen AN, Kammermeier C, et al. Incretin combination therapy for the treatment of non-alcoholic steatohepatitis. Diabetes Obes Metab 2020;22:1328–1338
9. Coskun T, Sloop KW, Loghin C, et al. LY3298176, a novel dual GIP and GLP-1 receptor agonist for the treatment of type 2 diabetes mellitus: from discovery to clinical proof of concept. Mol Metab 2018;18:3–14
10. Frias JP, Nauck MA, Van J, et al. Efficacy and safety of LY3298176, a novel dual GIP and GLP-1 receptor agonist, in patients with type 2 diabetes: a randomised, placebo-controlled and active comparator-controlled phase 2 trial. Lancet 2018;392:2180–2193
11. Selvaraju RK, Velikyan I, Johansson L, et al. In vivo imaging of the glucagonlike peptide 1 receptor in the pancreas with 68Ga-labeled DO3A-exendin-4. J Nucl Med 2013;54:1458–1463
12. Nalin L, Selvaraju RK, Velikyan I, et al. Positron emission tomography imaging of the glucagon-like peptide-1 receptor in healthy and streptozotocin-induced diabetic pigs. Eur J Nucl Med Mol Imaging 2014;41:1800–1810
13. Eriksson O, Haack T, Hijazi Y, et al. Receptor occupancy of dual glucagon-like peptide 1/glucagon receptor agonist SAR425899 in individuals with type 2 diabetes. Sci Rep 2020;10:16758
14. Velikyan I, Haack T, Bossart M, et al. First-in-class positron emission tomography tracer for the glucagon receptor. EJNMMI Res 2019;9:17
15. Eriksson O, Velikyan I, Haack T, et al. Assessment of glucagon receptor occupancy by Positron Emission Tomography in non-human primates. Sci Rep 2019;9:14960
16. Sherman SK, Carr JC, Wang D, O'Dorisio MS, O'Dorisio TM, Howe JR. Gastric inhibitory polypeptide receptor (GIPR) is a promising target for imaging and therapy in neuroendocrine tumors. Surgery 2013;154:1206–1213; discussion 1214
17. Sherman SK, Maxwell JE, Carr JC, et al. GIPR expression in gastric and duodenal neuroendocrine tumors. J Surg Res 2014;190:587–593
18. Reubi JC, Fourmy D, Cordomi A, Tikhonova IG, Gigoux V. GIP receptor: expression in neuroendocrine tumours, internalization, signalling from endosomes and structure-function relationship studies. Peptides 2020;125:170229
19. Reubi JC, Waser B. Triple-peptide receptor targeting in vitro allows detection of all tested gut and bronchial NETs. J Nucl Med 2015;56:613–615
20. Strosberg J, El-Haddad G, Wolin E, et al.; NETTER-1 Trial Investigators. Phase 3 trial of ^{177}Lu-dotatate for midgut neuroendocrine tumors. N Engl J Med 2017;376:125–135

21. Wild D, Bomanji JB, Benkert P, et al. Comparison of ^{68}Ga-DOTANOC and ^{68}Ga-DOTATATE PET/CT within patients with gastroenteropancreatic neuroendocrine tumors. J Nucl Med 2013;54:364–372

22. Brom M, Oyen WJ, Joosten L, Gotthardt M, Boerman OC. ^{68}Ga-labelled exendin-3, a new agent for the detection of insulinomas with PET. Eur J Nucl Med Mol Imaging 2010;37:1345–1355

23. Christ E, Wild D, Ederer S, et al. Glucagon-like peptide-1 receptor imaging for the localisation of insulinomas: a prospective multicentre imaging study. Lancet Diabetes Endocrinol 2013;1:115–122

24. Eriksson O, Velikyan I, Selvaraju RK, et al. Detection of metastatic insulinoma by positron emission tomography with [(68)ga]exendin-4-a case report. J Clin Endocrinol Metab 2014;99:1519–1524

25. Gourni E, Waser B, Clerc P, Fourmy D, Reubi JC, Maecke HR. The glucose-dependent insulinotropic polypeptide receptor: a novel target for neuroendocrine tumor imaging—first preclinical studies. J Nucl Med 2014;55:976–982

26. Willekens SMA, Joosten L, Boerman OC, Brom M, Gotthardt M. Characterization of ^{111}In-labeled glucose-dependent insulinotropic polypeptide as a radiotracer for neuroendocrine tumors. Sci Rep 2018;8:2948

27. Evers A, Pfeiffer-Marek S, Bossart M, et al. Multi-parameter peptide optimization towards stable triple agonists for the treatment of diabetes and obesity. Adv Therap 2020;3:2000052

28. Evers A, Haack T, Lorenz M, et al. Design of novel exendin-based dual glucagon-like peptide 1 (GLP-1)/glucagon receptor agonists. J Med Chem 2017; 60:4293–4303

29. Patlak CS, Blasberg RG. Graphical evaluation of blood-to-brain transfer constants from multiple-time uptake data. Generalizations. J Cereb Blood Flow Metab 1985;5:584–590

30. Selvaraju RK, Bulenga TN, Espes D, et al. Dosimetry of [(^{68})Ga]Ga-DO3A-VS-Cys(40)-Exendin-4 in rodents, pigs, non-human primates and human - repeated scanning in human is possible. Am J Nucl Med Mol Imaging 2015;5: 259–269

31. Cristy M, Eckerman K. *Specific Absorbed Fractions of Energy at Various Ages from Internal Photons Sources. ORNL/TM-8381 V1-V7*. Oak Ridge, TN, Oak Ridge National Laboratory, 1987

32. Eriksson O, Rosenström U, Selvaraju RK, Eriksson B, Velikyan I. Species differences in pancreatic binding of DO3A-VS-Cys^{40}-Exendin4. Acta Diabetol 2017;54:1039–1045

33. Adriaenssens AE, Biggs EK, Darwish T, et al. Glucose-dependent insulinotropic polypeptide receptor-expressing cells in the hypothalamus regulate food intake. Cell Metab 2019;30:987–996.e6

34. Yip RG, Boylan MO, Kieffer TJ, Wolfe MM. Functional GIP receptors are present on adipocytes. Endocrinology 1998;139:4004–4007

35. Schiellerup SP, Skov-Jeppesen K, Windeløv JA, et al. Gut hormones and their effect on bone metabolism. Potential drug therapies in future osteoporosis treatment. Front Endocrinol (Lausanne) 2019;10:75

36. Pappenheimer JR, Karnovsky ML, Maggio JE. Absorption and excretion of undegradable peptides: role of lipid solubility and net charge. J Pharmacol Exp Ther 1997;280:292–300